

ORIGINAL ARTICLE

Open Access

# Studying the penetration of fatty acids into human skin by ex vivo TOF-SIMS imaging

Toma Kezutyte<sup>1†</sup>, Nicolas Desbenoit<sup>2†</sup>, Alain Brunelle<sup>2\*</sup> and Vitalis Briedis<sup>1</sup>

## Abstract

Fatty acids classified as chemical penetration enhancers (CPEs) might cause the fluidization and perturbation of *stratum corneum* (SC) lipid matrix. The penetration of oleic, linoleic, lauric and capric acids into human skin was studied by time-of-flight secondary ion mass spectrometry (TOF-SIMS) imaging and related to fatty acids enhancing effect on lipophilic model drug tolnaftate penetration into human epidermis and dermis *ex vivo*. Fatty acid enhancing effect on tolnaftate penetration into human skin was evaluated using Bronaugh-type flow-through diffusion cells. After *in vitro* penetration studies visualization and spatial localization of fatty acid molecules in human skin were performed using TOF-SIMS. Penetration of oleic, linoleic, lauric and capric acids into human skin was compared to the control skin sections by ion images and intensity profiles. Only oleic acid significantly ( $P < 0.05$ ) enhanced tolnaftate penetration into epidermis (enhancing ratio equal to 1.867). CPE might have no effect on model drug penetration enhancement, but might penetrate itself into the skin.

**Keywords:** Stratum corneum, Fatty acids, Penetration enhancers, TOF-SIMS, Mass spectrometry imaging

## Background

*Stratum corneum* (SC), composed of corneocytes and extracellular lipid matrix, is recognized as the main barrier layer for passive diffusion of drug molecules into and through the skin. Knowledge about SC lipid organization allows for better understanding and interpretation of low permeability of drugs through SC and the modes of chemical penetration enhancers (CPEs) action. Fatty acids belong to lipophilic CPEs which might cause the reorganization of SC lipid matrix, thus the prerequisite for fatty acid enhancing effect on drug permeation would be its penetration into the skin and following disruption of skin lipids arrangement.

SC lipid matrix is mainly composed of neutral lipids: ceramides (CER), cholesterol (CHOL) and free fatty acids (FFA) [1] in an approximate molar ratio 3:2:1 [2]. FFAs, naturally present in the SC, predominantly have saturated and straight chains of 22 (docosanoic acid), 24 (lignocerin acid) and 26 (hexacosanoic acid) carbon atoms [3,4]. Oleic and linoleic acids are the only unsaturated fatty acids detected in SC [5]. Freeze-fracture

[6,7] and ruthenium tetroxide post-fixation [8] electron microscopy studies revealed that lipids are arranged into bilayers [9,10]. Lipid chains tend to pack in tight lateral highly ordered packing (according to packing density: liquid < hexagonal (gel) < orthorhombic (crystalline) phases), which has been studied using atomic force microscopy [11], Fourier transformed infrared spectroscopy [12], wide-angle X-ray diffraction [13] and electron diffraction [14]. All three phases coexist, but it is believed that conformationally ordered orthorhombic packing of lipids is mainly responsible for the resistance to transdermal delivery of molecules [15].

Small-angle X-ray diffraction [16-18] and electron microscopy [19,20] studies demonstrated that two lamellar structures, namely long and short periodicity phases (LPP and SPP, respectively), are characteristic to lamellar ordering of lipid bilayers [21]. Lipid lamella is oriented in parallel to corneocyte surface and its LPP has a repeat distance of 13 nm and SPP – of 6 nm [22]. LPP is organized in trilamellar repeat units of broad-narrow-broad electron lucent bands [23] and is considered to highly impact SC barrier properties. Several theoretical SC lipid model systems were proposed in order to describe the ordering of lipids in lamella. These models, such as the stacked monolayer model (proposed by Swartzendruber

\* Correspondence: Alain.Brunelle@icsn.cnrs-gif.fr

†Equal contributors

<sup>2</sup>Centre de Recherche de Gif, Institut de Chimie des Substances Naturelles, CNRS, Gif-sur-Yvette, France

Full list of author information is available at the end of the article

et al., 1989 [20]), the domain mosaic model (Forslind, 1994 [24]), the sandwich model (Bouwstra et al., 2000 [18]) and single gel phase model (Norlen, 2001 [25]) comprise the architecture of lipid molecules arrangement and the phase behaviour of lipid matrix [26,27].

Lamellar but not lateral lipid organization is dependent on pH [28], thus pH is also maintaining human skin barrier capacity and is in the range of 4.0-5.5 [29].

Well-defined SC lipid composition, organization and phase behaviour of extracellular matrix allow for better interpretation of CPE interactions with lipid molecules. In order to relate the penetration of oleic, linoleic, lauric and capric fatty acids and their enhancing effect on lipophilic model drug penetration into human skin *ex vivo*, two techniques were applied: *in vitro* skin penetration studies and mass spectrometry imaging (MSI). *In vitro* skin penetration studies were carried out using Bronaugh-type flow-through diffusion cells. Donor solutions containing model drug and CPE dissolved were applied to the skin surface for 12 h. Model drug was quantified in skin layers using a validated HPLC-UV method. The enhancing ratio of fatty acid on model drug's penetration was calculated. In order to demonstrate the penetration of CPE into human skin, MSI was applied after *in vitro* skin penetration studies. Among the various techniques aiming to map the surface of the sample, MSI is the only analytical method capable of providing in a single run the spatial distribution of a wide range of molecules over the surface of a biological sample [30]. Time-of-flight secondary ion mass spectrometry (TOF-SIMS) is a technique of choice for MSI and to our knowledge there is no published data on any attempts to visualize exogenously applied fatty acids penetration and distribution in human skin till now. This technology consists of the bombardment of the sample by a beam of mono- or polyatomic ions, which induce desorption/ionization of secondary ions from the sample surface [31-35]. It also offers the possibility to localize various molecules, mainly lipids and metabolites, with a mass-to-charge ratio up to  $m/z$  1000-1500 and a lateral resolution from 400 nm to 1-2  $\mu\text{m}$ , which makes the technology particularly efficient for the analysis of tissue sections. The field of research of TOF-SIMS imaging is then rapidly expanding and more widely used in many applications, mainly in biological sciences and medicine [36-39]. In the present work, we have used TOF-SIMS imaging in order to visualize and evaluate the penetration of externally applied fatty acids into human skin.

As enhancing effect of fatty acids was investigated, a lipophilic model drug with appropriate physicochemical properties ensuring its penetration via lipoidal route had to be chosen. A thiocarbamate antifungal drug tolnaftate

was selected as a model compound for *in vitro* skin penetration experiments. High hydrophobicity ( $XLogP = 5.5$ ), low molecular weight (307.4 Da) and melting point of 109-112°C (Eur. Pharm. 6.0; 01/2008:1158) are physicochemical properties which ensure tolnaftate's capability of passive diffusion through SC via lipoidal intercellular route and accumulation in superficial layers of skin. Hydrophilic skin layers form a barrier to tolnaftate deeper penetration.

## Methods

### Chemicals and reagents

Tolnaftate (O-naphthalen-2-yl methyl(3-methylphenyl) thiocarbamate; Eur. Pharm. 6.0; purity of 99.7%) was obtained from pharmaceutical company Sanitas AB (Kaunas, Lithuania) as a gift. Polyethylene glycol 400 (PEG 400) was purchased from Carl Roth GmbH (Karlsruhe, Germany). Capric acid (decanoic acid) was obtained from Merck Schuchardt OHG (Hohenbrunn, Germany). Oleic acid (cis-9-octadecenoic acid) and methanol (Chromasolv<sup>®</sup>) were purchased from Sigma-Aldrich Chemie GmbH (Steinheim, Germany). Linoleic acid (cis, cis-9,12-octadecadienoic acid) and lauric acid (dodecanoic acid) were purchased from Alfa Aesar GmbH (Karlsruhe, Germany). Sodium azide ( $\text{NaN}_3$ ) was obtained from POCh (Gliwice, Poland). Ethanol (96.3%) was obtained from Stumbras AB (Kaunas, Lithuania). All other reagents were of analytical grade.

### Human skin preparation

Studies with human skin were approved by Kaunas Region Bioethical Committee. Caucasian women's (of age 25-40) abdominal skin was obtained after excision in the Department of Plastic and Reconstructive Surgery, Hospital of Lithuanian University of Health Sciences Kaunas Clinics, appropriately treated and stored at -20°C for not longer than 6 months before use.

### Equipment

*In vitro* skin penetration experiments were carried out using teflon-made Bronaugh-type flow-through diffusion cells. Acceptor medium was circulated by peristaltic pump (Masterflex<sup>®</sup> L/S<sup>®</sup>, Cole-Parmer Instrument Co., Illinois, USA). Extraction of skin layers was performed using Bandelin Sonorex Digitec Ultrasonic Bath (DT 156, Bandelin electronic GmbH & Co. KG, Berlin, Germany).

HPLC analysis was carried out using Shimadzu Liquid Chromatograph (Shimadzu Corporation, Kyoto, Japan) coupled with UV-vis detector.

### Preparation of the donor phase

The donor solutions for *in vitro* skin penetration experiments were prepared by dissolving tolnaftate (1%,

w/w) in PEG 400 and following addition of oleic, linoleic, lauric or capric acid to comprise 10% (w/w) of total amount. If necessary, slight heating (up to 50°C) was employed. Tolnaftate 1% (w/w) solution in PEG 400 was used as control.

#### ***In vitro* skin penetration experiments**

Full-thickness human skin was mounted into Bronaugh-type flow-through diffusion cells (diffusional area 0.64 cm<sup>2</sup>). 37±1°C was maintained in temperature controlled block, holding the cells. 12 h equilibration period was followed circulating 0.9% NaCl+0.005% NaN<sub>3</sub> underneath the skin. Infinite dose (approximately 200 mg) of donor solutions was applied on the SC side of the skin surface for another 12 h. The acceptor fluid (4 mL 0.9% NaCl+0.005% NaN<sub>3</sub>) was pumped at a rate of 0.6 mL/min and was entirely replaced after 4 and 8 h. After 12 h the donor phase was carefully removed and the skin surface was rinsed with ethanol (96.3%) and then 0.9% NaCl.

After *in vitro* skin penetration experiment skin specimens were analyzed for tolnaftate content in epidermis and dermis separately, using a validated HPLC method [40], or were frozen and subjected to TOF-SIMS imaging analysis.

#### **HPLC analysis of human skin layers for model drug content**

After *in vitro* skin penetration experiments epidermis was separated from dermis using dry heat separation method [41]. Separated layers were extracted with methanol, following bath sonication for 30 min. The supernatant was filtered through nylon membrane filter (0.45 µm, Carl Roth GmbH, Karlsruhe, Germany) and injected into HPLC.

Separation of tolnaftate from endogenous compounds of skin matrix was accomplished on a LiChrospher<sup>®</sup> 100 RP-18 Endcapped column, 125 × 4 mm, i.d., packed with 5 µm size particles (Merck KGaA, Darmstadt, Germany) and maintained at 40°C. A LiChrospher 100 RP-18e (5 µm) (LiChroCART 4–4) was used as a guard column. The flow rate of the mobile phase (70% methanol and 30% bi-distilled water) was 0.8 mL/min and the injection volume was 10 µL. Tolnaftate detection was set at λ = 257 nm.

#### **TOF-SIMS imaging of human skin sections for CPE penetration visualization and ion imaging**

Circle full-thickness skin specimens, obtained after *in vitro* skin penetration experiments, were immediately frozen at -60°C and stored until cryosectioning procedure. Skin specimens were embedded in OCT medium and sections of 12 µm thick were cut at -20°C using a CM3050-S cryostat (Leica Microsystems SA, Nanterre,

France) and immediately deposited on a silicon wafer (2-in.-diameter polished silicon wafers, ACM, Villiers-Saint-Frédéric, France). The samples were dried under vacuum at a pressure of a few hectopascals for 15 min before analysis. Optical images were recorded with an Olympus BX51 microscope (Olympus, Rungis, France) equipped with lenses ×1.25 to ×50 and a ColorView I camera, monitored by Cell<sup>B</sup> software (Soft Imaging System, GmbH, Münster, Germany).

The experiments were performed using a commercial TOF-SIMS IV time-of-flight mass spectrometer (ION-TOF GmbH, Münster, Germany), located at the Institut de Chimie des Substances Naturelles (CNRS, Gif-sur-Yvette, France). The spectrometer is equipped with a liquid metal ion gun (LMIG) filled with bismuth. Bi<sup>+</sup> cluster ions were selected for all experiments. Primary ions extracted from the source emitted with a 25 kV potential reach the sample surface with a kinetic energy of 25 keV and at angle of incidence of 45°. Secondary ions are accelerated to an energy of 2 keV, fly through a field free region, and are reflected with a single stage reflector (effective flight path ~ 2 m) before being post accelerated to 10 keV just before hitting the entrance surface of the hybrid detector, which is made of one single micro-channel plate, followed by a scintillator and a photomultiplier. A low-energy electron flood gun is activated between two primary ions pulses in order to neutralize the sample surface with the minimum damage [42].

Only one mode of operation of the primary ion column has been used during the experiments, which is called 'high-current bunched mode' [43,44], thus providing both a beam focus of 2 µm and a pulse duration of a less 1 ns. Such experimental conditions enabled an excellent mass resolution,  $M/\Delta M = 8000$  (full width at half maximum, FWHM), at  $m/z$  500. The Bi<sup>+</sup> primary ion current, measured at 10 kHz with a Faraday cup on the grounded sample holder, is ~0.65 pA in the high-current bunched mode. For images of human skin sections, a large-area analysis (1.5 mm × 0.5 mm) was performed using these same LMIG conditions, i.e. high-current bunched mode, and the so-called stage scan. In this case, the sample is moved step by step to record three successive patches of 0.5 mm × 0.5 mm each. The number of pixel was 750 × 250, each pixel having a size 2 × 2 µm<sup>2</sup>. Under these conditions, the fluence (also called primary ion dose density) is maintained to 5 × 10<sup>11</sup> ions/cm<sup>2</sup>, which is below the so-called static SIMS limit [45].

Because of the very low kinetic energy distribution of the secondary ions, the relationship between the time-of-flight and the square root of  $m/z$  is always linear over the whole mass range. The calibration was always internal, and signals used for initial calibration were those of H<sup>-</sup>, C<sup>-</sup>, CH<sup>-</sup>, CH<sub>2</sub><sup>-</sup>, C<sub>2</sub><sup>-</sup>, C<sub>3</sub><sup>-</sup>, and C<sub>4</sub>H<sup>-</sup> for the negative ion mode.

The data acquisition and processing software was SurfaceLab 6.2 (ION-TOF GmbH, Münster, Germany).

### Statistical analysis

For the statistical analysis, one-way analysis of variance (ANOVA) together with Tukey's HSD test were applied using SPSS software. The level of significance was determined as  $P < 0.05$ .

## Results

### Effect of fatty acids on tolnaftate penetration into epidermis

The amounts of tolnaftate (T) ( $\mu\text{g}/\text{cm}^2$ ,  $n=3$ ) penetrating into epidermis from control solution and 10% (w/w) fatty acid solutions during 12 h of *in vitro* skin penetration experiments were assessed by HPLC-UV and are presented in Table 1. The enhancing effect of fatty acid on tolnaftate penetration into 1  $\text{cm}^2$  of epidermis (E) was expressed as the enhancing ratio (ER) and calculated using the following formula:

$$ER = \frac{T \text{ amount in E from formulation with fatty acid } (\mu\text{g}/\text{cm}^2)}{T \text{ amount in E from control formulation } (\mu\text{g}/\text{cm}^2)}$$

The obtained ER values are presented in Table 1.

ANOVA revealed that tolnaftate amount penetrating into 1  $\text{cm}^2$  of epidermis from the solution containing oleic acid was significantly greater ( $P < 0.05$ ) than from the control solution. Linoleic, lauric and capric acids did not significantly enhance tolnaftate penetration into epidermis comparing to the control.

Tolnaftate was not penetrating into hydrophilic dermis (only traces below limit of quantitation were found) and no drug was detected in the acceptor fluid.

### TOF-SIMS imaging of fatty acids penetration into human skin

Human skin sections were analyzed by TOF-SIMS imaging to demonstrate the penetration of fatty acids into

**Table 1 Amount of tolnaftate in human epidermis quantified by a validated HPLC-UV method, and enhancing ratios of fatty acids**

Donor phase	T amount, $\mu\text{g}/\text{cm}^2 \pm \text{SD}$ , $n=3$ (epidermis)	ER (epidermis)
Control solution	$2.56 \pm 0.15$	-
With 10% oleic acid	$4.77 \pm 0.79$	1.86*
With 10% linoleic acid	$2.61 \pm 0.32$	1.02
With 10% lauric acid	$3.06 \pm 0.32$	1.20
With 10% capric acid	$2.42 \pm 0.40$	0.95

Abbreviations: T, tolnaftate; ER, enhancing ratio.

\*Significant difference at  $P < 0.05$ .

skin. Fatty acids are labeled (CX:Y), which specifies the number of carbon atoms (X) and double bonds (Y) in the molecule. Figure 1 shows a typical mass spectrum recorded in the negative ion mode. This spectrum is dominated by lipid ion peaks, mainly fatty acids. The most intense ion peaks together with their formula are listed in Table 2. Human skin sections in depth of 1500  $\mu\text{m}$  contained whole epidermis and part of dermis. Indeed, the epidermis layer is about 100  $\mu\text{m}$ , while the dermis is about 1000  $\mu\text{m}$  in thickness. On the other hand, during the skin penetration studies hydrophilic dermis gets swollen due to acceptor medium, circulated underneath the skin.

Together with optical images of the sections, Figure 2 shows ion images corresponding to the spatial localization of  $[\text{M-H}]^-$  carboxylate ions of capric acid C10:0 ( $m/z$  171.10, top left), lauric acid C12:0 ( $m/z$  198.96, top right), linoleic acid C18:2 ( $m/z$  279.28, bottom left), and oleic acid C18:1 ( $m/z$  281.29, bottom right), in human skin treated with 10% fatty acid solution (b, e, h and k, respectively) and control (c, f, i and l, respectively). The ion images for each fatty acid have been normalized according to the higher  $mc$  value, in order to allow for direct comparison. For all these figures, optical images (a, d, g and j) are those of human skin sections corresponding to the ion images (b, e, h and k). TOF-SIMS analyses were repeated in triplicate for each fatty acid exposed tissue in order to confirm the analytical repeatability and the biological reproducibility (Additional file 1: Figure S1).

TOF-SIMS imaging revealed that lauric (Figure 2e) and oleic (Figure 2k) acids significantly penetrate into human skin comparing to the control (Figure 2f and Figure 2l, respectively). Capric (Figure 2b) and linoleic (Figure 2h) acids show a penetration into the skin sections (Figure 2c and Figure 2i, respectively), which is not as significant as for lauric and oleic acids. These relative variations of concentration as a function of

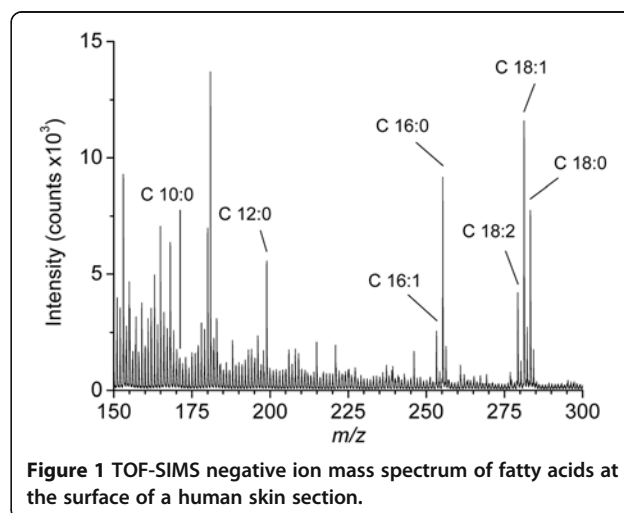


**Figure 1 TOF-SIMS negative ion mass spectrum of fatty acids at the surface of a human skin section.**

**Table 2 Mass-to-charge ratio of the main fatty acid carboxylate ions detected in the TOF-SIMS spectra in negative ion mode from the surface of sections from human skin and their chemical assignments**

Fatty acid name	M	<i>m/z</i> value of the [M-H] <sup>-</sup> ion
Capric acid	C <sub>10</sub> H <sub>20</sub> O <sub>2</sub> (C10:0)	171.091
Lauric acid	C <sub>12</sub> H <sub>24</sub> O <sub>2</sub> (C12:0)	198.959
Palmitoleic acid	C <sub>16</sub> H <sub>30</sub> O <sub>2</sub> (C16:1)	253.245
Palmitic acid	C <sub>16</sub> H <sub>32</sub> O <sub>2</sub> (C16:0)	255.261
Linoleic acid	C <sub>18</sub> H <sub>32</sub> O <sub>2</sub> (C18:2)	279.264
Oleic acid	C <sub>18</sub> H <sub>34</sub> O <sub>2</sub> (C18:1)	281.275

The labels (CX:Y) specifies the number of carbon atoms (X) and double bonds (Y) in the ion.

depth are not obviously observed directly from the images shown in Figure 2, particularly because the skin sections are not exempt from holes or lipid droplets. That is the reason why intensity profiles, as a function of depth, have been drawn from each of these fatty acid ion images (Figure 3). These intensity profiles are shown by a black solid line in the case of fatty acid exposed, and red solid line for the control. These profiles show the intensity of a specific ion species, over the whole analysed depth, and integrated over the entire width of the images. The results, which are presented in Figure 3, are from the same data acquisition as of Figure 2. If the solid black line lies above the red one, it could be concluded

that the corresponding fatty acid penetrates into the skin layers. It is clear from this figure that capric, oleic, linoleic and lauric acids did penetrate into skin when compared to the control. Furthermore, the lauric acid shows a high accumulation into the dermis when compared to the control. It must be noted that there is not comparable ion image corresponding to the tol-naftate drug molecule, because this active compound was not detected by TOF-SIMS imaging.

## Discussion

Combination of *in vitro* skin penetration method and TOF-SIMS imaging allowed relating the CPE effect on model drug diffusion into the skin during 12 h experiment with enhancer capability to enter the skin layers.

The diffusion cell method is a reliable method for measuring drug transport into/across the skin. In our studies, human skin was obtained from the same donor, thus inter-individual variance was reduced and the coefficients of variation (CV) were lower than 16.6% (calculations made after determination of tol-naftate levels in skin layers by HPLC).

TOF-SIMS analysis of skin specimens might be interfered by several factors. Normally, skin surface is covered by sebum, composed of squalene, wax esters and triglycerides [28]. Lipases acting on the surface of SC hydrolyze the sebaceous lipids to FFAs of C16 and

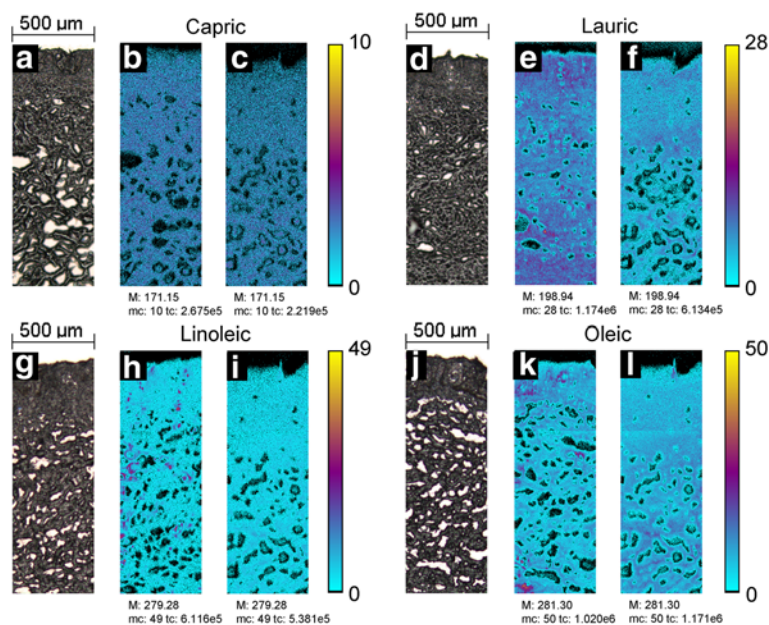


**Figure 2 Optical and mass spectrometry images of human skin sections. a, d, g and j:** Optical pictures of transversal human skin sections; **b, e, h and k:** TOF-SIMS images (negative ion mode) showing lateral distribution of capric, lauric, linoleic and oleic acid ions in skin treated with 10% fatty acid solution; **c, f, i and l:** TOF-SIMS images (negative ion mode) showing lateral distribution of capric, lauric, linoleic and oleic acid ions in control skin. Field of view 1.5 × 0.5 mm<sup>2</sup>, 750 × 250 pixels, pixel size 2 × 2 μm<sup>2</sup>, fluence 5 × 10<sup>11</sup> ions/cm<sup>2</sup>. The amplitude of the color scale corresponds to the maximum number of counts *mc* and could be read as [0, *mc*]. *tc* is the total number of counts recorded for the specified *m/z* (the sum of counts in all pixels).

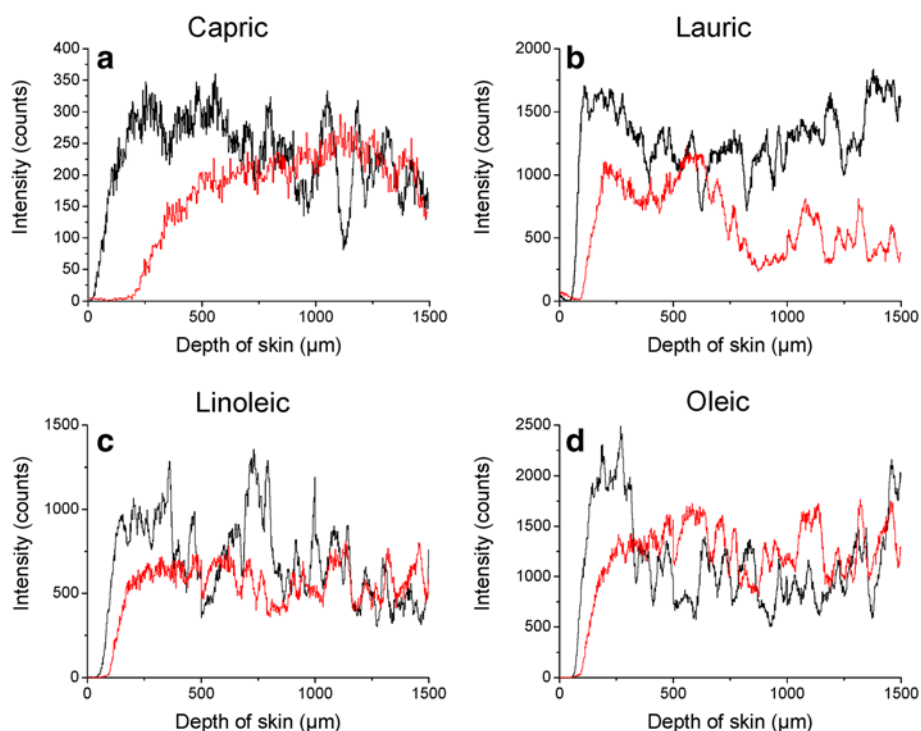


**Figure 3** Average ion intensities of the different fatty acids as a function of depth in the human skin sections for: top left capric acid (a), top right lauric acid (b), bottom left linoleic acid (c), bottom right oleic acid (d). Each viewgraph presents a combination of both experiments: 10% fatty acid in PEG 400 (solid black lines) and control (solid red lines). Note that depth of skin could not be associated to *in vivo* conditions as swelling of skin occurs in diffusion cells due to absorption of acceptor medium, circulating underneath the skin sample.

C18 with monounsaturations or branched chains [29]. Lauric and sapienic (C16:1) acids deriving from triglycerides (TGC) and covering the surface of human skin, are associated with antimicrobial action [46]. Thus FFAs naturally present on skin surface might affect the TOF-SIMS analysis of externally applied fatty acids. In this case SC surface wipe procedures before and after *in vitro* skin penetration experiments are important for validity of results. Cleaning of SC surface with 0.9% NaCl before *in vitro* experiments and careful removal of donor phase followed by rinsing with ethanol and 0.9% NaCl after *in vitro* experiments, ensured elimination of sebum traces from skin surface.

On the other hand, cryosectioning of skin specimens for TOF-SIMS analysis caused contamination of skin sections with TGC from subcutaneous fat [29]. The contamination with lipid droplets was visually observed in microscopic examination of skin samples and TOF-SIMS analysis revealed, that in these lipid droplets oleic, linoleic, palmitic and palmitoleic acids were present. Despite above mentioned factors, TOF-SIMS analysis allowed for ion imaging and evaluation of fatty acid penetration into human skin after *in vitro* skin penetration experiments and valuable and reliable results were obtained.

Lipophilic CPEs cause fluidization and perturbation of SC lipid matrix as they partition and insert the

hydrophobic tails into highly ordered packing of lipid bilayers. Differences in CPE head group and CER or CHOL structure [47] cause disruption of crystalline lipid packing. Formation of microcavities in SC lipids and increase of free volume fraction cause the enhancement of drugs diffusion coefficient [48] and, according to Fick's first law of diffusion, promotion of the permeation of molecules through SC occurs [49].

The enhancing effect of aliphatic acids has a parabolic dependence on chain length: the maximum effect is exerted by fatty acids with chain lengths around C12 [50,51]. Lauric acid has a high affinity to skin due to its optimal partition coefficient and solubility parameter [52] and it also might acquire a spatial form, which is conformationally similar to CHOL framework and which affects the packing of lipids [51]. During 12 h of *in vitro* skin penetration experiment, lauric acid penetrated into human skin from PEG 400 solution, but its enhancing effect on tolnaftate penetration was not significant.

Kravchenko et al. [51] states, that acids with shorter chains of less than C11 are not capable to disturb the packing of lipids in SC, as short chain acids are insufficiently lipophilic [53]. On the other hand, Nair and Panchagnula [47] proposed, that C10-C12 chain length acids disrupt CER-CHOL or CHOL-CHOL interaction and in this way should increase the permeability of drugs.

In our experiments capric acid penetrated into skin, but probably did not cause rearrangement of lipids and thus did not significantly enhance the penetration of tolnaftate.

Oleic and linoleic acids are both unsaturated, having one and two double bonds, respectively. Central location of double bond conditions the formation of a 'kink' [50], and this is attributed to the most potential CPE – oleic acid. Oleic acid is considered to create fluid-like phase within intercellular space [54-57]. In our studies, oleic acid significantly enhanced tolnaftate penetration into epidermis (ER=1.867) and its penetration into human skin was confirmed by TOF-SIMS analysis. Linoleic acid did not have a significant enhancing effect on tolnaftate penetration, while its penetration was confirmed by TOF-SIMS imaging.

## Conclusions

TOF-SIMS imaging of oleic, linoleic, lauric and capric acids in human skin confirmed their penetration. In addition, only lauric acid indicates a high accumulation in the dermis. On the other hand, only oleic acid demonstrated significant enhancing effect on hydrophobic model drug penetration. Penetration of fatty acid itself could not be considered as sufficient prerequisite for enhancing the penetration of model drug. Differences in physicochemical properties of fatty acids might determine their different affinity to skin lipids and mechanisms of action, thus their penetration capabilities and enhancing effect on lipophilic model drug penetration are different.

In order to alter skin barrier properties, CPEs are widely used in dermatological products as it is a simple and convenient way to improve drug's penetration. It is common to evaluate the CPE's effect on drug penetration into the skin while performing *in vitro* skin penetration studies. But if enhancer does not have any effect on drug penetration, it does not mean that enhancer itself is not penetrating into the skin and that no possible toxicity, pharmacological response or irreversibility of action could be associated with it. The need of analytical method, suitable for fast and reproducible mapping of enhancer directly on biological tissue without any sample preparation, might be overcome by using TOF-SIMS imaging.

## Additional file

**Additional file 1: TOF-SIMS images (negative ion mode) showing the lateral distribution of capric (top left), lauric (top right), linoleic (bottom left) and oleic acid (bottom right) ions in skin treated with 10% fatty acid solution.** Field of view  $1.5 \times 0.5 \text{ mm}^2$ ,  $750 \times 250$  pixels, pixel size  $2 \times 2 \mu\text{m}^2$ , fluence  $5 \times 10^{11}$  ions/cm<sup>2</sup>. The amplitude of the color scale corresponds to the maximum number of counts *mc* and could be read as  $[0, mc]$ . *tc* is the total number of counts recorded for the specified *m/z* (the sum of counts in all pixels).

## Competing interests

The authors declare that they have no competing interest.

## Authors' contributions

TK, ND, AB, VB. Performed the experiments: TK, ND. Analyzed the data: ND. Wrote the paper: TK, ND, AB, VB. All the authors read and approved the final manuscript.

## Author details

<sup>1</sup>Department of Clinical Pharmacy, Lithuanian University of Health Sciences, Kaunas, Lithuania. <sup>2</sup>Centre de Recherche de Gif, Institut de Chimie des Substances Naturelles, CNRS, Gif-sur-Yvette, France.

Received: 12 December 2012 Accepted: 26 December 2012

Published: 6 February 2013

## References

1. Feingold KR (2007) The role of epidermal lipids in cutaneous permeability barrier homeostasis. *J Lipid Res* 48:2531–2546
2. Kuempel D, Swartzendruber DC, Squier CA, Wertz PW (1998) In vitro reconstitution of stratum corneum lipid lamellae. *Biochim Biophys Acta* 1372:135–140
3. Kessner D, Kiselev M, Dante S, Haub T, Lersch P, Wartewig S, Neubert RHH (2008) Arrangement of ceramide [EOS] in a stratum corneum lipid model matrix: new aspects revealed by neutron diffraction studies. *Eur Biophys J* 37:989–999
4. Bouwstra JA, Honeywell-Nguyen PL (2002) Skin structure and mode of action of vesicles. *Adv Drug Deliv Rev* 54:S41–S55
5. Vicanova J, Ponec M, Weerheim A, Swope V, Westbrook M, Harriger D, Boyce S (1997) Epidermal lipid metabolism of cultured skin substitutes during healing of full-thickness wounds in athymic mice. *Wound Repair Regen* 5:329–338
6. Craane-Van Hinsberg IW, Verhoef JC, Spies F, Bouwstra JA, Gooris GS, Junginger HE, Bodde HE (1997) Electroperturbation of the human skin barrier in vitro: II. Effects on stratum corneum lipid ordering and ultrastructure. *Microsc Res Tech* 37:200–213
7. Breathnach AS, Goodman T, Stolinski C, Gross M (1973) Freeze-fracture replication of cells of stratum corneum of human epidermis. *J Anat* 114:65–81
8. Van Der Meulen J, Van Den Bergh BAI, Mulder AA, Mommaas AM, Bouwstra JA, Koerten HK (1996) The use of vibratome sections for the ruthenium tetroxide protocol: a key for optimal visualization of epidermal lipid bilayers of the entire human stratum corneum in transmission electron microscopy. *J Microsc* 184:67–70
9. Bouwstra JA, Gooris GS, Cheng K, Weerheim A, Bras W, Ponec M (1996) Phase behavior of isolated skin lipids. *J Lipid Res* 37:999–1011
10. Rissmann R, Oudshoorn MHM, Hennink WE, Ponec M, Bouwstra JA (2009) Skin barrier disruption by acetone: observations in a hairless mouse skin model. *Arch Dermatol Res* 301:609–613
11. Chen YL, Wiedmann TS (1996) Human stratum corneum lipids have a distorted orthorhombic packing at the surface of cohesive failure. *J Invest Dermatol* 107:15–19
12. Harrison JE, Groundwater PW, Brain KR, Hadgraft J (1996) Azone<sup>®</sup> induced fluidity in human stratum corneum. A fourier transform infrared spectroscopy investigation using the perdeuterated analogue. *J Contr Release* 41:283–290
13. White SH, Mirejovsky D, King GI (1988) Structure of lamellar lipid domains and corneocyte envelopes of murine stratum corneum. An x-ray diffraction study. *Biochemistry* 27:3725–3732
14. Pilgram GSK, Engelsma-van Pelt AM, Oostergetel GT, Koerten HK, Bouwstra JA (1998) Study on the lipid organization of stratum corneum lipid models by (cryo-) electron diffraction. *J Lipid Res* 39:1669–1676
15. Damien F, Boncheva M (2010) The Extent of Orthorhombic Lipid Phases in the Stratum Corneum Determines the Barrier Efficiency of Human Skin In Vivo. *J Invest Dermatol* 130:611–614
16. Bouwstra JA, Gooris GS, van der Spek JA, Bras W (1991) Structural investigations of human stratum corneum by small-angle X-ray scattering. *J Invest Dermatol* 97:1005–1012
17. Bouwstra JA, Gooris GS, Bras W, Downing DT (1995) Lipid organization in pig stratum corneum. *J Lipid Res* 36:685–695
18. Bouwstra JA, Dubbelaar FER, Gooris GS, Ponec M (2000) The Lipid Organisation in the Skin Barrier. *Acta Derm-Venereol* 208:23–30
19. Elias PM, McNutt NS, Friend DS (1977) Membrane alterations during cornification of mammalian squamous epithelia: a freeze-fracture, tracer, and thin-section study. *Anat Rec* 189:577–594

20. Swartzendruber DC, Wertz PW, Kitko DJ, Madison KC, Downing DT (1989) Molecular models of the intercellular lipid lamellae in mammalian stratum corneum. *J Invest Dermatol* 92:251–257
21. McIntosh TJ (2003) Organization of Skin Stratum Corneum Extracellular Lamellae: Diffraction Evidence for Asymmetric Distribution of Cholesterol. *Biophys J* 85:1675–1681
22. de Jager M, Groenink W, Bielsa i Guivernau R, Andersson E, Angelova N, Ponec M, Bouwstra J (2006) A Novel *In Vitro* Percutaneous Penetration Model: Evaluation of Barrier Properties with P-Aminobenzoic Acid and Two of Its Derivatives. *Pharm Res* 23:951–960
23. Hill JR, Wertz PW (2003) Molecular models of the intercellular lipid lamellae from epidermal stratum corneum. *Biochim Biophys Acta* 1616:121–126
24. Forslind B (1994) A domain mosaic model of the skin barrier. *Acta Derm-Venerol* 74:1–6
25. Norlen L (2001) Skin Barrier Structure and Function: The Single Gel Phase Model. *J Invest Dermatol* 117:830–836
26. Kessner D, Ruettinger A, Kiselev MA, Wartewig S, Neubert RHH (2008) Properties of ceramides and their impact on the stratum corneum structure: a review; Part 2: Stratum corneum lipid model systems. *Skin Pharmacol Physiol* 21:58–74
27. Madison KC (2003) Barrier function of the skin: “La raison d’être” of the epidermis. *J Invest Dermatol* 121:231–241
28. Plasencia I, Norlen L, Bagattoli LA (2007) Direct Visualization of Lipid Domains in Human Skin Stratum Corneum’s Lipid Membranes: Effect of pH and Temperature. *Biophys J* 93:3142–3155
29. Norlen L, Plasencia I, Bagattoli L (2008) Stratum corneum lipid organization as observed by atomic force, confocal and two-photon excitation fluorescence microscopy. *Int J Cosmet Sci* 30:391–411
30. McDonnell LA, Heeren RMA (2007) Imaging mass spectrometry. *Mass Spectrom Rev* 26:606–643
31. Belu AM, Graham DJ, Castner DG (2003) Time-of-flight secondary ion mass spectrometry: techniques and applications for characterization of biomaterial surfaces. *Biomaterials* 24:3635–3653
32. Li T, Wu TD, Mazéas L, Toffin L, Guerquin-Kern JL, Leblon G, Bouchez T (2008) Simultaneous analysis of microbial identity and function using NanoSIMS. *Environ Microbiol* 10:580–588
33. Touboul D, Halgand F, Brunelle A, Kersting R, Tallarek E, Hagenhoff B, Laprèvote O (2004) Tissue Molecular Ion Imaging by Gold Cluster Ion Bombardment. *Anal Chem* 76:1550–1559
34. Touboul D, Kollmer F, Niehuis E, Brunelle A, Laprèvote O (2005) Improvement of Biological Time-of-Flight Secondary Ion Mass Spectrometry Imaging with a Bismuth Cluster Ion Source. *J Am Soc Mass Spectrom* 16:1608–1618
35. Sjövall P, Lausmaa J, Johansson B (2004) Mass Spectrometric Imaging of Lipid in Brain Tissue. *Anal Chem* 76:4271–4278
36. Brunelle A, Laprèvote O (2007) Recent Advances in Biological Tissue Imaging with Time-of-Flight Secondary Ion Mass spectrometry: Polyatomic Ion Sources, Sample Preparation, and Application. *Curr Pharm Design* 13:3335–3343
37. Brunelle A, Laprèvote O (2009) Lipid imaging with cluster time-of-flight secondary ion mass spectrometry. *Anal Bioanal Chem* 393:31–35
38. Nygren H, Malmberg P (2007) High resolution imaging by organic secondary ion mass spectrometry *Trends. Biotechnol* 25:499–504
39. Seyer A, Einhorn J, Brunelle A, Laprèvote O (2010) Localization of Flavanoids in Seeds by Cluster Time-of-Flight Secondary Ion Mass Spectrometry. *Anal Chem* 82:2326–2333
40. Kezutyte T, Kornysyova O, Maruska A, Briedis V (2010) Assay of tolnaftate in human skin samples after *in vitro* penetration studies using high performance liquid chromatography. *Acta Pol Pharm* 67:327–334
41. Kassis V, Søndergaard J (1982) Heat Separation of Normal Human Skin for Epidermal and Dermal Prostaglandin Analysis. *Arch Dermatol Res* 273:301–306
42. Gilmore IS, Seah MP (2002) Electron flood gun damage in the analysis of polymers and organics in time-of-flight SIMS. *Appl Surf Sci* 187:89–100
43. Sodhi RNS (2004) Time-of-flight secondary ion mass spectrometry (TOF-SIMS): versatility in chemical and imaging surface analysis. *Analyst* 129:483–487
44. Brunelle A, Touboul D, Laprèvote O (2005) Biological tissue imaging with time-of-flight secondary ion mass spectrometry and cluster ion sources. *J Mass Spectrom* 40:985–999
45. Vickerman JC (2001) In: Vickerman JC, Briggs D (ed). *TOF-SIMS-Surface analysis by Mass Spectrometry, Surface Spectra and IM Publications*, Manchester and Chichester
46. Drake DR, Brogden KA, Dawson DV, Wertz PW (2008) Thematic review series: skin lipids. Antimicrobial lipids at the skin surface. *J Lipid Res* 49:4–11
47. Nair VB, Panchagnula R (2003) Effect of iontophoresis and fatty acids on permeation of Arginine Vasopressin through rat skin. *Pharmacol Res* 47:563–569
48. Benson HAE (2005) Transdermal Drug Delivery: Penetration Enhancement Techniques. *Curr Drug Delivery* 2:23–33
49. Moser K, Kriwet K, Naik A, Kalia YN, Guy RH (2001) Passive skin penetration enhancement and its quantification *in vitro*. *Eur J Pharm Biopharm* 52:103–112
50. Marjukka Suhonen T, Bouwstra JA, Urtili A (1999) Chemical enhancement of percutaneous absorption in relation to stratum corneum structural alterations. *J Contr Release* 59:149–161
51. Kravchenko IA, Larionov VB, Aleksandrova AI, Ovcharenko NV, Polishchuk AA, Andronati SA (2003) Effect of skin permeability enhancers on the transdermal introduction of phenazepam studied *in vitro*. *Pharm Chem J* 37:369–373
52. Ogiso T, Shintani M (1990) Mechanism of the enhancement effect of fatty acids on the percutaneous absorption of propranolol. *J Pharm Sci* 79:1065–1071
53. Chisty MNA, Bellantone RA, Taft DR, Plakogiannis FM (2002) *In Vitro* Evaluation of the Release of Albuterol Sulfate from Polymer Gels: Effect of Fatty Acids on Drug Transport Across Biological Membranes. *Drug Dev Ind Pharm* 28:1221–1229
54. Boncheva M, Damien F, Normand V (2008) Molecular organization of the lipid matrix in intact Stratum corneum using ATR-FTIR spectroscopy. *Biochim Biophys Acta* 1778:1344–1355
55. Rowat AC, Kitson N, Thewalt JL (2006) Interactions of oleic acid and model stratum corneum membranes as seen by <sup>2</sup>H NMR. *Int J Pharm* 307:225–231
56. Ammar HO, Ghorab M, El-Nahhas SA, Kamel R (2007) Evaluation of chemical penetration enhancers for transdermal delivery of aspirin. *Asian J Pharm Sci* 2:96–105
57. Ongpipattanukul B, Burnette RR, Potts RO, Francoeur ML (1991) Evidence that Oleic Acid Exists in a Separate Phase Within Stratum Corneum Lipids. *Pharm Res* 8:350–354

doi:10.1186/1559-4106-8-3

**Cite this article as:** Kezutyte et al.: Studying the penetration of fatty acids into human skin by ex vivo TOF-SIMS imaging. *Biointerphases* 2013 8:3.

**Submit your manuscript to a SpringerOpen® journal and benefit from:**

- Convenient online submission
- Rigorous peer review
- Immediate publication on acceptance
- Open access: articles freely available online
- High visibility within the field
- Retaining the copyright to your article

Submit your next manuscript at ► [springeropen.com](http://springeropen.com)